Preprints, 4th IFAC Conference on
Advances in Proportional-Integral-Derivative Control
Almería, Spain | June 12-14, 2024

Transient Response Analysis of Reset PID Control Systems ⋆

Xinxin Zhang[1*] **S. Hassan HosseinNia**[1**]

[1] *Department of Precision and Microsystems Engineering (PME), Delft University of Technology, Mekelweg 2, Delft, The Netherlands (e-mails: X.Zhang-15@tudelft.nl *, S.H.HosseinNiaKani@tudelft.nl **).*

Abstract: Reset controllers have demonstrated their efficacy in enhancing transient responses, such as the overshoot and response time in motion control systems. Designing these systems to meet specific transient requirements requires a method for analyzing transient responses. However, the inherent nonlinearity of reset control systems presents challenges in this regard, limiting their widespread application. This study introduces a novel method for analyzing the step responses of closed-loop reset control systems. By decomposing the step response of the reset system into piece-wise functions, with each piece-wise function computed based on linear systems, this analysis method offers new insights into understanding reset systems. Experimental validation conducted on eleven reset Proportional-Integral-Derivative (PID) control systems implemented on a precision motion stage confirms the effectiveness of the proposed method. The experimental results also underscore the applicability of the method as a tool for selecting optimized parameters and reset control structures to achieve enhanced transient responses.

Keywords: Reset Control System, Transient Response, Precision Motion, Reset PID.

1. INTRODUCTION

In high-precision industries, the demand for superior transient response, such as shorter response times and reduced overshoot, is escalating. Linear controllers, notably the Proportional-Integral-Derivative (PID), have been employed in industries for decades Safa et al. (2018). However, linear controllers face inherent limitations, such as the Bode magnitude-phase relationship and the waterbed effect (Saikumar et al. (2021)). This prompts the exploration of nonlinear controllers capable of overcoming these constraints to meet evolving industrial requirements.

The reset controller is a hybrid system that combines a linear controller with a resetting mechanism. The first reset element termed as the Clegg Integrator (CI), incorporates the "Zero-crossing law" into a linear integrator (Clegg (1958)). The "Zero-crossing law" allows the CI's output to reset to zero when the input signal crosses zero. The first-order harmonic in the CI exhibits a 52° phase lead compared to that of the linear integrator without compromising the gain benefits, thus breaking the conventional Bode phase-gain relationship. Following the CI, various reset elements have emerged, including the First-order reset element (FORE), Second-order reset element (SORE), Constant in gain Lead in phase (CgLp), hybrid integrator-gain systems (Higs) (see Horowitz and Rosenbaum (1975); Krishnan and Horowitz (1974); Beker et al. (2004); Baños and Vidal (2007); Deenen et al. (2017); Saikumar et al. (2019).

Previous studies have explored the application of reset controllers to improve transient responses. In Li et al. (2011), reset controllers were designed to achieve shorter settling times and lower overshoot compared to linear controllers in hard disk drives. Zhao et al. (2019) achieved non-overshoot performance by applying the FORE structure, and Banos and Vidal (2012) demonstrated that the Proportional-Integral + Clegg Integrator (PI+CI) structure achieved less overshoot and settling time while maintaining the response velocity of a first-order plus dead-time system. To apply reset control systems effectively for improved transient response, precise analysis methods are required. Various approaches have been explored, including rule-of-thumb methods for enhancing settling (transient) performance in Beerens et al. (2019) and numerical analysis for tuning one specific reset element in mechanical motion systems in Karbasizadeh and HosseinNia (2022).

However, explicit and precise methods for analyzing the transient response of the reset control system remain unexplored, primarily due to the nonlinearity inherent in reset control system. This paper addresses this gap by introducing a novel linear-based analytical method for analyzing the step response of Single-Input Single-Output (SISO) reset control systems with a single reset state. The proposed method separates the step responses of SISO reset control systems into piece-wise functions, with each function analysed based on linear calculations. Experimental validation on a precision motion stage demonstrates the efficacy of the proposed method. Moreover, the illustrative examples demonstrate the applicability of the new method in tuning parameters and selecting reset control structures to achieve improved transient performance.

The paper is organized into five sections. Section 2 provides fundamental backgrounds on reset control systems. Section 3 introduces the linear-based method for analyzing the transient response of reset control systems. Section 4 presents experimental validations of the new methods using eleven reset control systems on a precision motion

⋆ This work was not supported by any research agency.

stage. Finally, Section 5 concludes the paper, emphasizing the novelty of the introduced method, its practical applicability, and potential future research.

2. BACKGROUND

The block diagram of a closed-loop reset control system is shown in Fig. 1, including a reset controller denoted by the block $\mathcal{C}(s)(s = j\omega,\ j = \sqrt{-1})$, a linear controller $\mathcal{C}_\alpha(s)$, and a plant represented by the block $\mathcal{P}(s)$.

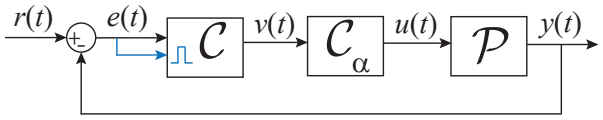

Fig. 1. The block diagram of the reset control system, where $r(t)$, $e(t)$, $v(t)$, $u(t)$, and $y(t)$ are the reference input, error, reset output, control input, and system output, respectively. The blue lines represent the reset action.

The reset controller $\mathcal{C}(s)$ is a hybrid time-invariant system that integrates the "zero-crossing law" (Banos and Barreiro (2012); Guo and Chen (2019)), allowing the state of the controller to reset to zero when the input signal of the reset controller crosses zero. In practice, the zero-crossing instants can be detected using algorithms such as those presented in Copp and Sanfelice (2016). The set J of reset instant t_i is defined as $J := \{t_i | e(t_i) = 0, i \in \mathbb{N}\}$. The state-space representative for a SISO reset controller $\mathcal{C}$ is described as follows:

$$\mathcal{C} = \begin{cases} \dot{x}_r(t) = A_R x_r(t) + B_R e(t), & \text{when } t \notin J, \\ x_r(t^+) = A_\rho x_r(t), & \text{when } t \in J, \\ v(t) = C_R x_r(t) + D_R e(t). \end{cases} \tag{1}$$

In this context, $x_r(t) \in \mathbb{R}^{n_c}$ represents the state of the reset controller, where n_c is the number of reset controller states. The state-space matrices A_R, B_R, C_R, and D_R constitute the base linear controller, denoted as $\mathcal{C}_{bl}$. The Fourier-domain transfer function of $\mathcal{C}_{bl}$ is given by

$$C_{bl}(\omega) = C_R(j\omega I - A_R)^{-1} B_R + D_R. \tag{2}$$

The base-linear system (BLS) of the reset control system in Fig. 1 is defined as the system replacing the reset controller $\mathcal{C}$ by its base-linear controller $\mathcal{C}_{bl}$. The open-loop transfer function of the base-linear system is defined as

$$\mathcal{L}_{bl}(\omega) = \mathcal{C}_{bl}(\omega)\mathcal{C}_\alpha(\omega)\mathcal{P}(\omega). \tag{3}$$

The second equation pertains to the dynamic of the reset controller at the reset instant t_i, where $e(t_i) = 0$. A_ρ is the reset matrix:

$$A_\rho = \begin{bmatrix} A_{\rho\gamma} & \\ & I_{n_l} \end{bmatrix}, A_{\rho\gamma} = \text{diag}(\gamma_1, \gamma_2, \cdots, \gamma_i, \cdots, \gamma_{n_r}), \tag{4}$$

where γ_i $(1 \le i \le n_r \in \mathbb{N})$ characterises the reset ratio within the range of $(-1, 1)$. The subscript n_l and n_r pertain to the number of linear states and reset states, respectively, with the total number of states being $n_c = n_r + n_l$. In this study, our focus is on the reset controller with a single reset state. Specifically, in A_ρ as given in (4), we have $A_{\rho\gamma} = \gamma$ and $n_r = 1$. The reset controller with a single reset state includes examples such as the CI, the FORE, and the SORE with resetting the first state.

In Fig. 1, the linear controller $\mathcal{C}_\alpha$ combined with the plant $\mathcal{P}$ is defined as $\mathcal{P}_\alpha = \mathcal{C}_\alpha\mathcal{P}$. The state-space representation of $\mathcal{P}_\alpha$ is defined as:

$$\mathcal{P}_\alpha = \begin{cases} \dot{x}_\alpha(t) = A_\alpha x_\alpha(t) + B_\alpha v(t), \\ y_\alpha(t) = C_\alpha x_\alpha(t), \end{cases} \tag{5}$$

where $x_\alpha \in \mathbb{R}^{n_\alpha \times 1}$ is the state of $\mathcal{P}_\alpha$ with the number of $n_\alpha \in \mathbb{N}$.

Combining (1) and (5), the state-space representative of the reset control system without inputs is given by

$$\mathcal{H} = \begin{cases} \dot{x}(t) = A_{cl} x(t), & x \notin J, \\ x(t^+) = A_{\rho cl} x(t), & x \in J, \\ y(t) = C_{cl} x(t), \end{cases} \tag{6}$$

where

$$A_{cl} = \begin{bmatrix} A_R & -B_R C_\alpha \\ B_\alpha C_R & A_\alpha \end{bmatrix}. \tag{7}$$

In (6), $x^T = [x_c{}^T\ x_\alpha{}^T] \in \mathbb{R}^{n_s \times 1}$ represents the state of the reset control system $\mathcal{H}$, with the number of $n_s = n_c + n_\alpha$.

The reset system (6) is quadratically stable if it satisfies the H_β condition as follows (Banos and Barreiro (2012)): There exists a $\beta \in \mathbb{R}^{n_r \times 1}$ and a positive definite matrix $P_{n_r} \in \mathbb{R}^{n_r \times n_r}$ such that the transfer function

$$H_\beta(s) \triangleq [P_{n_r}\ 0_{n_r \times n_l}\ \beta C_\alpha](sI - A_{cl})^{-1} \times [I_{n_r \times n_r}\ 0_{n_l \times n_r}\ 0_{n_\alpha \times n_r}]^T \tag{8}$$

is strictly positive real.

According to findings from Dastjerdi et al. (2022), to ensure uniformly exponentially convergent behavior in reset control systems, the following assumption is made:

Assumption 1. The reset controller is under the zero initial condition, there is an infinite number of reset instants t_i with $\lim_{t_i \to \infty} = \infty$, the reset system satisfies the H_β condition (8), and the reset input signal $e(t)$ is a Bohl function.

Note that this assumption can be achieved through design considerations, such as in Saikumar et al. (2021); Banos and Barreiro (2012); Samad et al. (2019).

3. THE STEP RESPONSE ANALYSIS OF RESET CONTROL SYSTEMS

This section introduces a novel method for analyzing the step response of a reset control system by decomposing the step responses into piece-wise functions. First, the first piece function is the same as that of the base-linear system. Then, Lemma 2 provides the expression for the second piece function. Subsequently, Theorem 3 introduces the algorithm to compute the entire step responses.

Define a normalized step signal as

$$h(t) := \begin{cases} 1, & t > 0, \\ 0, & t \le 0, \end{cases} \tag{9}$$

whose Fourier transform is $H(\omega) = \mathscr{F}[h(t)] = 1/(j\omega)$.

The step response of the reset control system depicted in Fig. 1 is defined as the output $y(t)$ under the input signal $r(t) = |R|h(t)$, $|R| \in \mathbb{R}^+$. Specifically, for the base-linear system (BLS), the step response is denoted as $y_{bl}(t)$.

Additionally, the signals $x_{bl}(t)$, $v_{bl}(t)$, $u_{bl}(t)$, and $e_{bl}(t)$ represent the base-linear state, reset output, control input, and error signals of the BLS, respectively.

In a control system, the rise time is the duration it takes for a signal to transition from a specified low value to a specified high value. Let $t_0 = 0$ denote the initial time. The time instant t_i (where $i \in \mathbb{Z}^+$) denotes the i-th reset instant, satisfying $e(t_i) = 0$ in the reset control system. In the step response of the reset control system illustrated in Fig. 1 under the input signal $r(t) = |R|h(t)$, we define the rise time as $t_r = t_1$, which represents the time from t_0 to the time instant t_1 when $e(t)$ first reaches zero, determined by

$$e_{bl}(t_r) = 0, \tag{10}$$

where

$$\begin{aligned} \mathcal{S}_{bl}(\omega) &= 1/(1 + \mathcal{L}_{bl}(\omega)), \\ e_{bl}(t) &= |R|\mathscr{F}^{-1}[\mathcal{S}_{bl}(\omega)H(\omega)]. \end{aligned} \tag{11}$$

Note that since before t_r, there is no reset action, t_r functions as the rise time for both the reset control system and the BLS. During the time interval $[t_{i-1},\ t_i)$, the step response $y(t)$ is represented by its i-th piece $y_i(t)$. For instance, during the time interval $[0, t_r)$, the step response is expressed as $y_1(t) = y_{bl}(t)$.

Lemma 2. The step response of the reset control system depicted in Fig. 1 with the input $r(t) = |R|h(t)$, under Assumption 1, within the time interval $[t_r, t_2)$ is given by:

$$y_2(t) = y_{bl}(t) + (A_\rho - I)x_{bl}(t_r)h_\alpha(t - t_r),\ t \in [t_r, t_2), \tag{12}$$

where

$$\begin{aligned} x_{bl}(t) &= |R|\mathscr{F}^{-1}[\Phi_{bl}(\omega)H(\omega)], \\ y_{bl}(t) &= |R|\mathscr{F}^{-1}[\mathcal{T}_{bl}(\omega)H(\omega)], \\ h_\alpha(t) &= \mathscr{F}^{-1}[R_\delta(\omega)\mathcal{T}_\alpha(\omega)H(\omega)], \\ \Phi_{bl}(\omega) &= (j\omega I - A_R)^{-1}B_R\mathcal{S}_{bl}(\omega), \\ R_\delta(n\omega) &= C_R(jn\omega I - A_R)^{-1}jn\omega I, \\ \mathcal{T}_\alpha(\omega) &= \mathcal{C}_\alpha(\omega)\mathcal{P}(\omega)/(1 + \mathcal{L}_{bl}(\omega)), \\ \mathcal{T}_{bl}(\omega) &= \mathcal{C}(\omega)\mathcal{C}_\alpha(\omega)\mathcal{P}(\omega)/(1 + \mathcal{L}_{bl}(\omega)), \end{aligned} \tag{13}$$

in which $H(\omega) = \mathscr{F}[h(t)]$ is given in (9).

Proof. Utilizing (1), the state of the BLC $\mathcal{C}_{bl}$ in the closed-loop BLS in Fig. 1 under a unit step input $|R|h(t)$, is given by

$$\begin{aligned} x_{bl}(t) &= |R|\mathscr{F}^{-1}[\Phi_{bl}(\omega)H(\omega)], \\ \Phi_{bl}(\omega) &= (j\omega I - A_R)^{-1}B_R\mathcal{S}_{bl}(\omega). \end{aligned} \tag{14}$$

The first reset instant of the reset system occurs at the rise time $t_r = t_1$, determined by (10) and (11). According to (1), at the reset instant t_r, we have

$$x_r(t_r^+) = A_\rho x_r(t_r) = A_\rho x_{bl}(t_r). \tag{15}$$

From (15), at the time instant t_r, the reset action introduces a pulse signal denoted as $x_\delta(t)$, given by:

$$x_\delta(t) = x_r(t_r^+) - x_r(t_r) = (A_\rho - I)x_{bl}(t_r)\delta(t - t_r), \tag{16}$$

where $\delta(t)$ is a Dirac delta function.

From (16), during the time interval $[t_r, t_2)$, the state $x_r(t)$ of the reset controller is equal to the base-linear state output $x_{bl}(t)$ plus a step signal $x_{nl}(t)$, as depicted in Fig. 2, expressed as:

$$\begin{aligned} x_r(t) &= x_{bl}(t) + x_{nl}(t), \\ x_{nl}(t) &= h(t - t_r)[x_r(t_r^+) - x_r(t_r)] \\ &= h(t - t_r)(A_\rho - I)x_{bl}(t_r). \end{aligned} \tag{17}$$

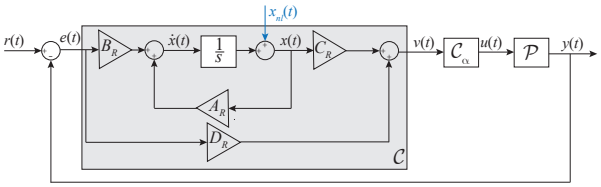

Fig. 2. The state-space-based block diagram of the reset control system in Fig. 1.

Let

$$v_{nl}(t) = v(t) - v_{bl}(t). \tag{18}$$

Figure 2 shows the state-space-based block diagram of the reset control system in Fig. 1. Based on the block diagram transformation principles Graybeal (1951), the signal $x_{nl}(t)$ is transformed into the signal $v_{nl}(t)$ by filtering it through the transfer function $R_\delta(\omega)\mathcal{S}_{bl}(\omega)$, where $R_\delta(\omega)$ and $\mathcal{S}_{bl}(\omega)$ are defined in (13) and (11), respectively. This process is mathematically expressed as:

$$v_{nl}(t) = \mathscr{F}^{-1}[R_\delta(\omega)\mathcal{S}_{bl}(\omega)X_{nl}(\omega)], \tag{19}$$

where $X_{nl}(\omega) = \mathscr{F}[x_{nl}(t)]$.

Combining equations (17) and (19), $v_{nl}(t)$ during the time interval $[t_r, t_2)$ is expressed as:

$$\begin{aligned} h_\delta(t) &= \mathscr{F}^{-1}[R_\delta(\omega)\mathcal{S}_{bl}(\omega)H(\omega)], \\ v_{nl}(t) &= h_\delta(t - t_r)(A_\rho - I)x_{bl}(t_r). \end{aligned} \tag{20}$$

Then, utilizing (18), (20), and the relationship between $v(t)$ and $y(t)$ depicted in the block diagram of Fig. 2, within the interval $[t_r, t_2)$, the output $y_2(t)$ is given by:

$$y_2(t) = y_{bl}(t) + y_{nl}(t), \tag{21}$$

where

$$\begin{aligned} y_{bl}(t) &= |R|\mathscr{F}^{-1}[\mathcal{T}_{bl}(\omega)H(\omega)], \\ y_{nl}(t) &= h_\alpha(t - t_r)(A_\rho - I)x_{bl}(t_r), \end{aligned} \tag{22}$$

in which $\mathcal{T}_{bl}(\omega)$ and $h_\alpha(t)$ are given in (13).

Here, the proof is concluded.

Theorem 3 extends the calculation for the step response during $[t_r, t_2)$ in Lemma 2 to the entire time domain.

Theorem 3. The step response $y(t)$ of a SISO reset control system with a single reset state to the input $r(t) = |R|h(t)$ and under Assumption 1, as illustrated in Fig. 1, manifests as a piece-wise signal, segmented by its reset instants t_i. The computation of $y(t)$ can be performed through the Algorithm 3.1:

Algorithm 3.1 Step response $y(t)$ of reset control systems.

1. $t_1 = t_r$ where t_r is the first solution of $y_{bl}(t) = |R|$.
2. During $(0,\ t_1)$, $y_1(t) = y_{bl}(t)$ and $x_r(t) = x_{bl}(t)$.
3. i = 1.
4. $x_{nl}^{i+1}(t_i) = (A_\rho - I)x_r(t_i)$.
5. $x_r(t) = x_r(t) + h_s(t - t_i)x_{nl}^{i+1}(t_i)$[a]
6. $y_{i+1}(t) = y_i(t) + h_\alpha(t - t_i)x_{nl}^{i+1}(t_i)$.
7. **Solve** $y_{i+1}(t) - |R| = 0$, and obtain its first zero t_{i+1}.
8. $i = i + 1$.
9. **Repeat from step 4, until** $\max\{|y_{i+1}(t) - y_i(t)|\} \le \epsilon$[b]

[a] $h_s(t) = \mathscr{F}^{-1}[\mathcal{S}_{bl}(\omega)H(\omega)]$.
[b] ϵ is the maximum absolute error set for the calculation.

If the system is unstable or not convergent, the step 9 in Algorithm 3.1 will be infinitely repeated. Stability and

convergence are not the focus of this paper and can be achieved through suitable design, so we won't delve into them extensively.

Proof. Similar to the process described from (15) to (17) in the proof for Lemma 2, at any arbitrary reset instant t_i, the reset action introduces a new pulse signal with an amplitude of $(A_\rho - I)x_r(t_i)$ to the state $x_r(t)$. This pulse signal is represented as a step signal $x_{nl}^{i+1}(t)$ within the interval $[t_i,\ t_{i+1})$, as expressed in Step 4 and given by:

$$x_{nl}^{i+1}(t) = (A_\rho - I)x_r(t_i)h(t - t_i). \tag{23}$$

As depicted in Fig. 2, during the time interval $[t_i,\ t_{i+1})$, the signal $x_{nl}^{i+1}(t)$ contributes to the $(i+1)$-th state output $x_{i+1}(t)$ through the transfer function $\mathcal{S}_{bl}(\omega)$. It also contributes to the $(i+1)$-th output $y_{i+1}(t)$ through the transfer function $R_\delta(\omega)\mathcal{T}_\alpha(\omega)$ based on Lemma 2. Consequently, steps 5 and 6 are derived. The subsequent steps involve iterative procedures to determine the next reset instant and introduce a new pulse signal until the step response reaches a steady-state. Here, the proof is concluded.

Definition 4. The overshoot in the step response $y(t)$ of the reset control system under the input $r(t) = |R|h(t)$ is defined as:

$$M_p\% = (\max\{y(t)\} - |R|)/|R|\%,\ \max\{y(t)\} > |R|. \tag{24}$$

The calculation outlined in Algorithm 3.1 is based on linear systems. If the step response function of the linear system is known, this algorithm can be applied to compute the step response of the reset control system analytically.

The existing literature suggests various methods for model reduction to achieve a second-order system representation, such as the Dominant Pole Approximation method Obinata and Anderson (2012). By employing model reduction methods, a Linear Time Invariant (LTI) system can be approximated as a second-order system. For instance, the reduced second-order system for the base-linear complementary sensitivity function $\mathcal{T}_{bl}(s)$ can be expressed as

$$\widetilde{\mathcal{T}'_{bl}}(s) = \frac{as^2 + bs + c}{ds^2 + es + f}. \tag{25}$$

Remark 5. By following the outlined procedure in Algorithm 3.1, essential transient response information for the reset control system, including t_r, t_p, and $M_p\%$, can be directly determined based on the reduced second-order system (25), using the following steps:

(1) First, for practical implementation, we utilize the "Model Reducer App" within MATLAB to derive the reduced second-order system $\mathcal{T}'_{bl}$ and $\mathcal{S}'_{bl}$, corresponding to $\mathcal{T}_{bl}$ in (13) and $\mathcal{S}_{bl}$ in (11) in the BLS. Then, utilizing step response analysis techniques tailored for second-order linear systems, as detailed in Nise (2020), we compute the base-linear output $\widetilde{y'_{bl}}(t_r)$ and the state $x'_{bl}(t_r)$ of the reduced systems with the input signal $r(t) = |R|h(t)$, using the equations in (13).
(2) Next, calculate the rise time of the reduced system, denoted as $\widetilde{t'_r}$, which is the time instant when $\widetilde{y'_{bl}}(t_r)$ first reaches the steady-state value of $|R|$, determined by $\widetilde{y'_{bl}}(t_r) = |R|$.
(3) Represent the first-piece step response within the interval $(0, \widetilde{t'_r})$ as $\widetilde{y'_1}(t) = \widetilde{y'_{bl}}(t)$.
(4) Determine the second-piece step response as $\widetilde{y'_2}(t) = \widetilde{y'_1}(t) + (A_\rho - I)x'_{bl}(t_r)\widetilde{h'_\alpha}(t - \widetilde{t'_r})$, for $t \in (\widetilde{t'_r}, \widetilde{t'_2})$. The time instant $\widetilde{t'_2}$ is determined by $\widetilde{y'_2}(\widetilde{t'_2}) = 0$, following the same process as the step 7 in Algorithm 3.1.
(5) Determine $\widetilde{h'_\alpha}(t)$ based on the reduced second-order system given by:
$$\widetilde{h'_\alpha}(t) = \mathscr{F}^{-1}[R_\delta(\omega)\widetilde{\mathcal{T}'_{bl}}(\omega)H(\omega)/\mathcal{C}_{bl}(\omega)]. \tag{26}$$
(6) The overshoot and peak time of the reduced system within the interval $[\widetilde{t'_r},\ \widetilde{t'_2})$ are denoted as $\widetilde{M'_p}\%$ and $\widetilde{t'_p}$, respectively. Determine $\widetilde{t'_p}$ and $\widetilde{M'_p}\%$ by calculating $\dot{\widetilde{y'_2}}(\widetilde{t'_p}) = 0$ and $\widetilde{M'_p}\% = |\widetilde{y'_2}(\widetilde{t'_p}) - |R||/|R| \cdot 100\%$.

The reliability of Remark 5 will be illustrated by providing a comparison between the parameters derived from the reduced system and practical measurements in Table 1 in Section 4.

4. ILLUSTRATIVE EXAMPLES

This section performs experimental validation for the proposed methods on reset PID control systems implemented on a precision motion stage.

4.1 Precision Positioning Setup

The "Spyder" precision positioning stage (in Fig. 3) is a planar motion system with 3 degrees of freedom. Three masses (M_1, M_2, M_3) are driven by three voice coil actuators (A_1, A_2, A_3) and employ a linear current source power amplifier. These masses utilize dual leaf flexures for exclusive connection to the base (M_c). Control systems are conducted on an NI compactRIO. The Mercury M2000 linear encoder ("Enc") sampled at 10 kHz and with 100 nm resolution senses mass positions. For this SISO study, only actuator A_1 positions mass M_1.

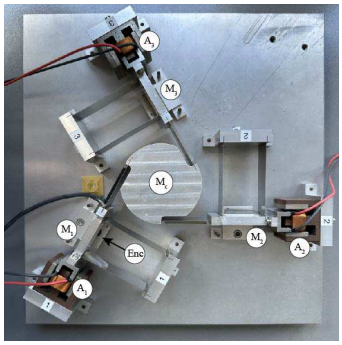

Fig. 3. The planar precision positioning system "Spyder".

Figure 4 shows the Frequency Response Function (FRF) of the setup, resembling a collocated double mass-spring-damper system with additional high-frequency parasitic dynamics. The "Spyder" system's transfer function in (27) is approximated as a single eigenmode mass-spring-damper model using Matlab's identification tool for control clarity.

$$\mathcal{P}(s) = \frac{6.615e5}{83.57s^2 + 279.4s + 5.837e5}. \tag{27}$$

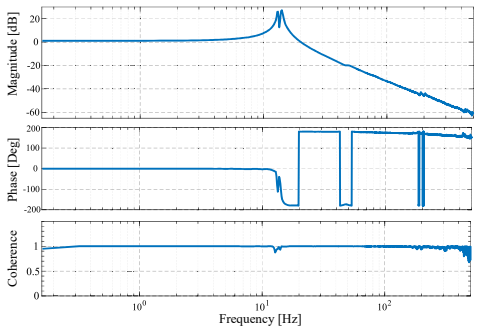

Fig. 4. FRF data from actuator A_1 to attached mass M_1.

4.2 Reset Control Systems

Figure 5(a) illustrates the block diagram of the Proportional-Clegg Integrator-PID (PCI-PID) control system. Figure 5(b) presents the structure of the CgLp-PI^{2}D controller, integrating the CgLp into the PI^{2}D systems. Here, the CgLp controller is a reset element that can provide phase lead without compromising gain advantages Saikumar et al. (2019).

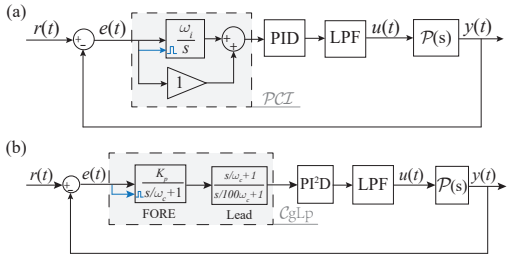

Fig. 5. (a) The PCI-PID and (b) the CgLp-PI^{2}D control system structures.

The parameters for these two systems are set as follows: $\omega_c = 240\pi$ [rad/s]; the Low-pass-filter (LPF) is defined as $1/(s/\omega_f + 1)$, with $\omega_f = 2400\pi$ [rad/s]. PI^{2}D is designed as $Kp(\omega_i/s + 1)^2(s/\omega_d + 1)/(s/\omega_t + 1)$, where $\omega_i = 24\pi$ [Hz]. In these two reset control systems, the Proportional-Derivative (PD) elements are tailored to achieve the desired crossover frequency (f_c) and phase margin (PM) in open-loop.

4.3 Transient Response Analysis Using The New Methods

Eleven reset control systems, applying PCI-PID and CgLp-PI^{2}D structures (in Fig. 5), are designed to achieve specified f_c and PM in Table 1. Systems $C_1 - C_4$ and $C_8 - C_{11}$ maintain a consistent f_c of 120 Hz and PM of 50°. Systems C_3, C_5, and C_6 share the same base-linear system with varying reset values (γ). System C_7 features a crossover frequency (f_c) of 200 Hz and a PM of 50°.

Definition 6. The experimental, Algorithm 3.1-predicted, and reduced second-order system predicted rise times are denoted as $\overline{t_r}$, $\widetilde{t_r}$, and $\widetilde{t'_r}$, respectively. The difference between $\overline{t_r}$ and $\widetilde{t'_r}$ is defined as $\widetilde{\epsilon'_r} = |\overline{t_r} - \widetilde{t'_r}|$. The corresponding groups of peak time and overshoot are defined as ($\overline{t_p}$, $\widetilde{t_p}$, $\widetilde{t'_p}$, $\widetilde{\epsilon'_p}$) and ($\overline{M_p}\%$, $\widetilde{M_p}\%$, $\widetilde{M'_p}\%$, $\widetilde{\epsilon'_M}\%$), respectively.

Figure 6 presents the predicted and experimental step responses for C_3, C_5, C_7, and C_{11}. The prediction and measurement data fit each other well. The quantitative transient specifications derived from both prediction and experiments, and the differences between experimental and reduced-model predicted values are listed in Table 1. Across cases $C_1 - C_{11}$, the prediction error for rise and peak time falls within the range of $(0.0001, 0.0004)$ and $(0.0002, 0.0011)$, respectively, with the largest error appearing in cases C_6 and C_3. The overshoot prediction error is within the range of $(0.5\%, 3.3\%)$, with the largest error occurring in the linear case C_8.

Results in Table 1 lead to the following conclusions:

(1) The proposed methods effectively predict reset control system step responses, offering a more efficient alternative to Simulink, with superior time efficiency and reduced configuration complexities compared to Simulink. Minor discrepancies between predictions and experiments may be attributed to external disturbances, setup variations, and system identification approximations. These variations are noticeable even in linear cases such as C_1 and C_8.
(2) Though $C_1 - C_4$ and $C_8 - C_{11}$ share the same bandwidth and phase margin in open-loop, their transient responses differ due to varying γ values. Case C_4 in the PCI-PID group and Case C_{11} in the CgLp-PI^{2}D group, with negative γ values, exhibit low overshoot with minimal compromise on peak time compared to cases with positive γ values and linear systems.
(3) Comparing the two control structures, PCI-PID and CgLp-PI^{2}D, both designed to have the same bandwidth and phase margin in open-loop, the PCI-PID structure displays lower overshoot and peak time. These findings highlight how the new analysis method can aid engineers in optimizing the selection of control structures to meet transient response specifications.

5. CONCLUSIONS

In conclusion, this paper introduces a method for analyzing the step responses of closed-loop reset control systems. The approach offers a fresh perspective by decomposing the step response of reset control systems into piece-wise linear functions. Experimental validation involving eleven reset PID control systems on a precision motion stage confirms the accuracy of the method.

In the illustrative examples, a negative reset value γ yields lower overshoot albeit with a minor compromise in peak time. Moreover, under the same open-loop phase margin and bandwidth, the PCI-PID configuration exhibits superior transient performance compared to the CgLp-PI^{2}D systems. These results underscore the abilities of the analysis method as a tool for control engineers to fine-tune and select optimized parameters in reset systems for enhanced transient responses. Future research endeavors will delve into a more comprehensive analytical representation and explore practical applications of this methodology.

REFERENCES

Banos, A. and Barreiro, A. (2012). *Reset control systems.* Springer.

Table 1. The parameters and transient specifications of reset control systems $C_1 - C_{11}$.

RC	Cases	f_c	PM	γ	$\overline{t_r}$ (s)	$\widetilde{t_r}$ (s)	$\widetilde{t'_r}$ (s)	$\widetilde{\epsilon'_r}$ (s)	$\overline{t_p}$ (s)	$\widetilde{t_p}$ (s)	$\widetilde{t'_p}$ (s)	$\widetilde{\epsilon'_p}$ (s)	$\overline{M_p}$%	$\widetilde{M_p}$%	$\widetilde{M'_p}$%	$\widetilde{\epsilon'_M}$%
PCI-PID	C_1	120	50	1	0.0020	0.0020	0.0021	0.0001	0.0033	0.0040	0.0041	0.0008	28.0%	30.3%	30.8%	2.8%
	C_2	120	50	0.5	0.0020	0.0021	0.0022	0.0002	0.0034	0.0040	0.0048	0.0008	28.0%	27.2%	27.5%	0.5%
	C_3	120	50	0	0.0021	0.0022	0.0023	0.0002	0.0033	0.0040	0.0044	0.0011	25.0%	24.6%	24.5%	0.5%
	C_4	120	50	-0.5	0.0025	0.0025	0.0026	0.0001	0.0040	0.0045	0.0049	0.0009	24.0%	23.0%	22.6%	1.4%
	C_5	139	45.2	-0.5	0.0021	0.0022	0.0023	0.0001	0.0032	0.0038	0.0042	0.0010	22.0%	21.2%	20.3%	1.7%
	C_6	112	43.8	0.5	0.0019	0.0022	0.0023	0.0004	0.0035	0.0042	0.0044	0.0009	28.0%	28.3%	28.8%	0.8%
	C_7	200	50	0	0.0013	0.0013	0.0014	0.0001	0.0024	0.0024	0.0026	0.0002	26.0%	25.9%	27.2%	1.2%
CgLp-PI^{2}D	C_8	120	50	1	0.0019	0.0020	0.0021	0.0003	0.0036	0.0036	0.0041	0.0005	34.0%	30.1%	30.7%	3.3%
	C_9	120	50	0.5	0.0018	0.0020	0.0020	0.0002	0.0041	0.0044	0.0046	0.0005	28.0%	31.0%	30.0%	2.0%
	C_{10}	120	50	0	0.0019	0.0020	0.0020	0.0001	0.0048	0.0048	0.0050	0.0002	28.0%	30.2%	27.2%	0.8%
	C_{11}	120	50	-0.5	0.0020	0.0021	0.0021	0.0001	0.0050	0.0053	0.0053	0.0003	26.0%	27.4%	22.8%	3.2%

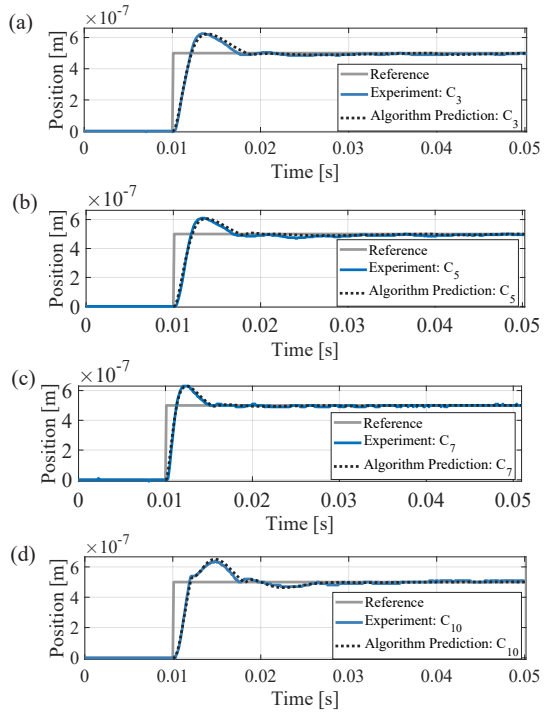

Fig. 6. Algorithm-predicted and experimental step responses for (a) C_3, (b) C_5, (c) C_7, and (d) C_{10}.

Baños, A. and Vidal, A. (2007). Definition and tuning of a pi+ ci reset controller. In *2007 european control conference (ECC)*, 4792–4798. IEEE.

Banos, A. and Vidal, A. (2012). Design of reset control systems: the pi+ ci compensator.

Beerens, R., Bisoffi, A., Zaccarian, L., Heemels, W., Nijmeijer, H., and van de Wouw, N. (2019). Reset integral control for improved settling of pid-based motion systems with friction. *Automatica*, 107, 483–492.

Beker, O., Hollot, C., Chait, Y., and Han, H. (2004). Fundamental properties of reset control systems. *Automatica*, 40(6), 905–915.

Clegg, J.C. (1958). A nonlinear integrator for servomechanisms. *Transactions of the American Institute of Electrical Engineers, Part II: Applications and Industry*, 77(1), 41–42.

Copp, D.A. and Sanfelice, R.G. (2016). A zero-crossing detection algorithm for robust simulation of hybrid systems jumping on surfaces. *Simulation Modelling Practice and Theory*, 68, 1–17.

Dastjerdi, A.A., Astolfi, A., Saikumar, N., Karbasizadeh, N., Valerio, D., and HosseinNia, S.H. (2022). Closed-loop frequency analysis of reset control systems. *IEEE Transactions on Automatic Control*, 68(2), 1146–1153.

Deenen, D., Heertjes, M.F., Heemels, W., and Nijmeijer, H. (2017). Hybrid integrator design for enhanced tracking in motion control. In *2017 American Control Conference (ACC)*, 2863–2868. IEEE.

Graybeal, T. (1951). Block diagram network transformation. *Electrical Engineering*, 70(11), 985–990.

Guo, Y. and Chen, Y. (2019). Stability analysis of delayed reset systems with distributed state resetting. *Nonlinear Analysis: Hybrid Systems*, 31, 265–274.

Horowitz, I. and Rosenbaum, P. (1975). Non-linear design for cost of feedback reduction in systems with large parameter uncertainty. *International Journal of Control*, 21(6), 977–1001.

Karbasizadeh, N. and HosseinNia, S.H. (2022). Continuous reset element: Transient and steady-state analysis for precision motion systems. *Control Engineering Practice*, 126, 105232.

Krishnan, K. and Horowitz, I. (1974). Synthesis of a non-linear feedback system with significant plant-ignorance for prescribed system tolerances. *International Journal of Control*, 19(4), 689–706.

Li, H., Du, C., and Wang, Y. (2011). Optimal reset control for a dual-stage actuator system in hdds. *IEEE/ASME Transactions on Mechatronics*, 16(3), 480–488.

Nise, N.S. (2020). *Control systems engineering*. John Wiley & Sons.

Obinata, G. and Anderson, B.D. (2012). *Model reduction for control system design*. Springer Science & Business Media.

Safa, A., Abdolmalaki, R.Y., and Nejad, H.C. (2018). Precise position tracking control with an improved transient performance for a linear piezoelectric ceramic motor. *IEEE Transactions on Industrial Electronics*, 66(4), 3008–3018.

Saikumar, N., Heinen, K., and HosseinNia, S.H. (2021). Loop-shaping for reset control systems: A higher-order sinusoidal-input describing functions approach. *Control Engineering Practice*, 111, 104808.

Saikumar, N., Sinha, R.K., and HosseinNia, S.H. (2019). "constant in gain lead in phase" element–application in precision motion control. *IEEE/ASME Transactions on Mechatronics*, 24(3), 1176–1185.

Samad, T., Mastellone, S., Goupil, P., van Delft, A., Serbezov, A., and Brooks, K. (2019). Ifac industry committee update, initiative to increase industrial participation in the control community. *Newsletters April 2019. IFAC*.

Zhao, G., Nešić, D., Tan, Y., and Hua, C. (2019). Overcoming overshoot performance limitations of linear systems with reset control. *Automatica*, 101, 27–35.